ADVANCED FUNCTIONAL MATERIALS
www.afm-journal.de

Multidimensional Data Encoding Based on Multicolor Microencapsulated Thermoresponsive Fluorescent Phase Change Materials

Jaume Ramon Otaegui, Daniel Ruiz-Molina, Jordi Hernando,* and Claudio Roscini**

Luminescent materials are emerging promising tools for digital data encoding due to their reduced cost, facile reading, robustness, and durability. For this, the use of fluorescent systems that combine multicolor emission with sensitivity to external stimuli will be highly desirable, as they can offer rewritable data encoding together with enhanced encryption security and storage density. Herein a novel strategy is pioneered to reach this goal, which exploits the temperature-responsive emission properties of the mixtures of regular fluorophores with simple organic phase change materials (PCMs) such as paraffins. By preparing a diversity of microcapsules of these mixtures comprising different dyes and PCMs, thermosensitive fluorescent pixels can be prepared in a low-cost, straightforward, and scalable manner that exhibits multicolor dynamic emission behavior. These features are capitalized to fabricate pixel arrays that perform two advanced digital encoding operations: high-security 3D information encryption, and 4D data storage.

1. Introduction

Hidden security luminescent marks that become visible upon photoexcitation lie at the core of major anticounterfeiting technologies in banknotes, identification documents, and valuable goods.[1–8] These are often simple labels for visual authentication, though more complex luminescent security elements can also be printed that encode information in a safer mode.[3–8] This is the case of 1D barcodes and 2D QR codes, encrypting binary data as variable emission printed line bars or 2D-pixel arrays, respectively.[9] Even higher-density information encoding can be achieved with multicolor luminescent 3D codes. In these systems, emission color is utilized as a third dimension to enhance the data density per unit area without significantly increasing the detection complexity.[10–14] This is achieved through the superposition of 2D luminescent arrays of pixels, each showing different possible emission colors.[9,11,15] As a result, 3D luminescent codes can provide extremely compact data storage in write-once-read-more documents,[16] while warranting superior information protection than conventional 2D codes.[17–19] To further boost these features, luminescent 3D codes can be made dynamic by introducing stimuli-responsive emissive materials in one or more of their pixels.[11,15,20–26] In this way, the information displayed can be varied reversibly or irreversibly upon application of external triggers, thus allowing for mutable data storage,[11,22,27,28] warning about the prior reading of the encoded data,[29,30] and incrementing the encryption-decryption security levels as the valuable data is only readable upon application of a very specific condition of an external stimulus.[23,31–34] To date, several types of materials have been used as 3D stimuli-responsive codes, including fluorescent polymers,[31] self-assembled fluorophores[32] and fluorescent host-guest systems,[35] luminescent metal-organic frameworks,[36] and carbon dots.[26] Among them, luminescent hydrogels are often preferred,[15,20,23,27,33] mainly due to their facile preparation,[37] high composition and stimuli sensitivity tunability,[15,38] and biocompatibility.[39,40] So far, good results have been reported for these systems, though the need for a co-solvent together with the complex miniaturization and printability of hydrogels might hamper their implementation in some anti-counterfeiting applications.[37]

Even denser data encoding can be achieved by monitoring the emission changes that occur in 3D codes over time during or after external stimulation (e.g., upon evaporation of a solvent,[35] during light-induced photoconversion,[41] or in the simplest scenario, after pulsed photoexcitation),[19,42,43] usually referred to as 4D codes.[35,41–43] However, this approach still suffers from several drawbacks: i) time is not an optimal dimension to store information compared to space or color due to the lack of control

J. R. Otaegui, D. Ruiz-Molina, C. Roscini
Catalan Institute of Nanoscience and Nanotechnology (ICN2)
CSIC and BIST
Campus UAB, Bellaterra, Barcelona 08193, Spain
E-mail: jaumeramon.otaegui@uab.cat; claudio.roscini@icn2.cat
J. R. Otaegui, J. Hernando
Departament de Química
Universitat Autònoma de Barcelona
Edifici C/n, Campus UAB, Cerdanyola del Vallès 08193, Spain
E-mail: jordi.hernando@uab.cat

The ORCID identification number(s) for the author(s) of this article can be found under https://doi.org/10.1002/adfm.202402510

DOI: 10.1002/adfm.202402510

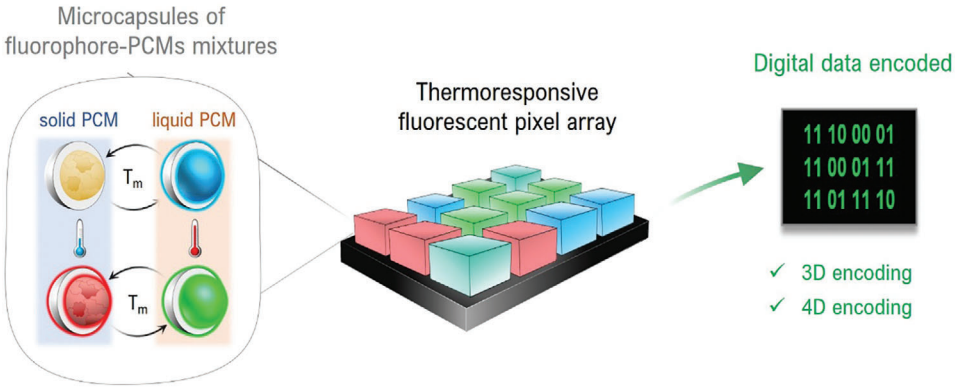

Figure 1. Scheme of our temperature-responsive fluorescent codes for 3D and 4D information encoding based on microencapsulated fluorophore-PCM mixtures loaded into polymer pixels. Highly dynamic multicolor emission behavior is accomplished in these systems by: i) mixing two types of MCs in the pixels that show spectrally separated thermosensitive fluorescence, and ii) utilizing MCs made from four paraffinic PCMs with different melting points, which therefore undergo luminescence switching at distinct temperatures.

in the scanning direction and speed; ii) time-dependent luminescence changes are generally continuous and, therefore, much more complex to detect than discrete and abrupt variations; and iii) emission changes rates are often dependent on the intensity of the applied stimulus (e.g., irradiation power), which makes them harder to be reproduced during independent readouts.

In light of these arguments, it would be highly preferred to develop novel stimuli-responsive luminescent 3D codes that combine low-cost, robustness, facile fabrication, scalability and transferability with reliable 4D information encoding – i.e, where (i) the fourth dimension for data encoding is defined by a non-time dependent and extensive stimulus that is easy to manipulate and scan (e.g., temperature, pH or voltage), and (ii) the emission changes produced are discrete rather than continuous.

Herein we hypothesize that thermosensitive fluorescent emitters incorporated in simple organic phase change materials (PCMs) such as paraffins, represent a promising strategy to reach these goals.[44–54] In such mixtures, the dyes can be abruptly and reversibly switched between two different supramolecular states (aggregated and non-aggregated) with different emission properties, a behavior that is controlled by the temperature-induced solid-to-liquid transition of the PCM.[44–54] Moreover, these mixtures can be properly structured as core-shell microcapsules (MCs) that can be incorporated in transparent polymers, acting as fluorescent pixels in thermoresponsive arrays. By combining MCs containing different fluorophores and paraffin within these pixels, highly dynamic multicolor emission can be accomplished, endowing the resulting arrays with high-security 3D data encoding properties as well as 4D storage capacity (**Figure 1**).

2. Results and Discussion

2.1. Temperature-Responsive Fluorescent Pixels Based on Microencapsulated Dye-PCM Mixtures

Dissolving regular fluorescent emitters in organic PCMs such as simple paraffins is a low-cost, straightforward, and versatile strategy for the preparation of temperature-responsive fluorescent materials.[44–54] By controlling the inter- and intramolecular interactions of the dispersed dyes through the solid–liquid transition of the surrounding matrix, these systems present two strikingly different luminescent states which can be interconverted by heating (or cooling) above (or below) PCM's melting point (T_m). Aiming for multicolor emission, two different commercially available emitters were selected in this work that could lead to thermoinduced fluorescence switching in well-separated spectral regions upon PCM phase transition: the blue emissive 9,10-bis(phenylethynyl)anthracene (BPEA), and the green emitting *N,N′*-bis(1-hexylheptyl)perylene-3,4,9,10-bis(dicarboximide) (PDI) (**Figure 2a**). Previous studies reported that PDI dispersed in paraffinic PCMs (e.g., eicosane, octacosane) at appropriate concentrations, exhibits an abrupt temperature-induced emission modulation.[50,52] Herein we reproduce such PDI behavior when dispersed in bulk docosane (DC), a different 22-carbon length paraffin with T_m = 42–45 °C.[55] For the resulting PDI@DC mixture (0.033 wt.%), a sudden on_1-on_2 switch from red excimer-like emission (Φ_{em} = 0.33) to green monomer fluorescence (Φ_{em} = 0.90) was measured upon solid-to-liquid transition of the paraffin (Figure S1a, Supporting Information). This thermoinduced emission switching would not occur in the absence of a phase change of the surrounding matrix, as PDI liquid solutions are known to undergo little fluorescence variation with temperature.[56] Therefore, it must be ascribed to the selective aggregation of the dye molecules that occurs in the solid state of the system, which is reverted upon paraffin melting (Figure S1b, Supporting Information). As BPEA is also known to alter its emissive properties upon self-aggregation,[57] a similar effect was anticipated for BPEA@DC mixtures. Indeed, a significant emission quenching was observed when BPEA was dispersed in solid bulk DC (0.05 wt.%, Φ_{em} = 0.12), while the bright blue-cyan emission of the monomeric dye could be recovered after DC melting (Φ_{em} = 0.95) – i.e., BPEA@DC exhibits off-on blue emission switching (Figure S2a, Supporting Information). This behavior cannot be ascribed to the thermal dependence of the intrinsic fluorescence quantum yield of BPEA, which has been reported to be nearly invariant with temperature in liquid solutions.[58] Instead, it must arise from the formation of low-emissive aggregates in solid DC, as confirmed by the broadening of the absorption spectrum of BPEA[57] that is in striking contrast with the narrower

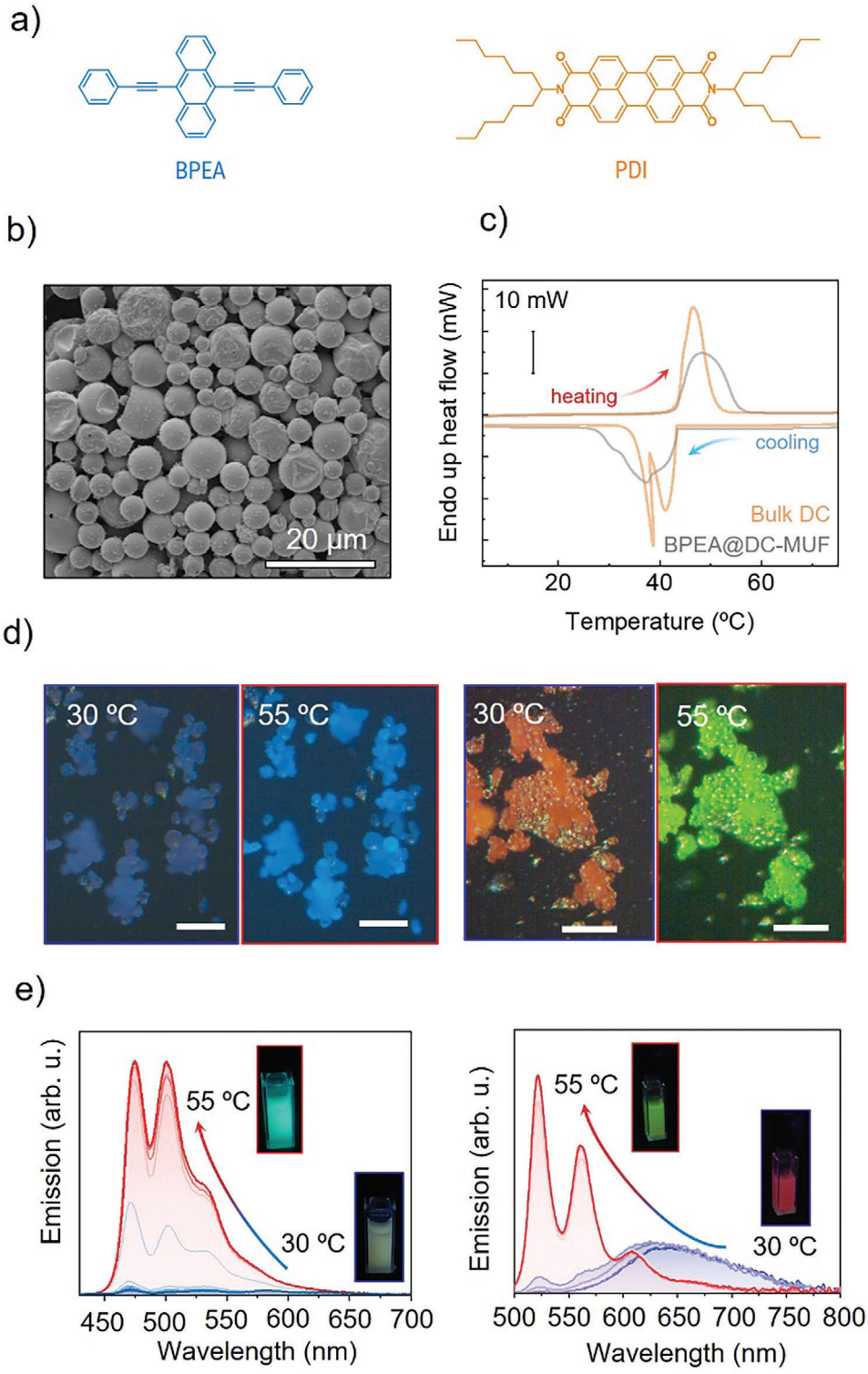

Figure 2. a) Molecular structures of BPEA and PDI. b) SEM image of PDI@DC-MUF MCs. c) DSC thermogram of bulk DC and BPEA@DC-MUF MCs (temperature ramp = 10 °C min^{-1}). d) Fluorescence microscopy images of (left) BPEA@DC-MUF and (right) PDI@DC-MUF at 30 and 55 °C (λ_{exc} = 365 nm). e) Variation of the fluorescence spectrum of (left) BPEA@DC-MUF and (right) PDI@DC-MUF with temperature from 30 to 55 °C (λ_{exc} = 445 nm). The insets show photographs of the colloidal aqueous suspensions of the corresponding MCs below (30 °C) and above (55 °C) DC T_m.

absorption bands recorded after DC melting (Figure S2b, Supporting Information).

To integrate different DC-fluorophore mixtures in the same pixels of 3D codes to obtain multicolor fluorescence, they were miniaturized into core-shell MCs. Melamine-urea-formaldehyde (MUF) was chosen as a polymeric shell for these MCs because of two principal reasons: its common use in industry for the encapsulation of thermochromic PCM-based systems;[59,60] and its high polarity, which must lead to good phase separation between the hydrophobic PCM-fluorophore core and the MUF shell, thus favoring the thermoresponsive fluorescence behavior of the initial bulk mixture to be preserved after encapsulation. BPEA- and PDI-containing MUF MCs were prepared following an adapted in situ polymerization methodology from the literature[61] (BPEA@DC-MUF and PDI@DC-MUF MCs, see the Supporting Information for further details). Scanning electron microscopy (SEM) analysis of the obtained materials confirmed that well-defined rounded-shaped microstructures were obtained with an average diameter size of ≈10.3 ± 4.0 µm (Figure 2b; Figure S3, Supporting Information). A clear phase transition at temperatures around DC T_m was identified in the differential scanning calorimetry (DSC) thermogram of the MCs, indicating the successful encapsulation of the PCM and the preservation of its thermal properties (Figure 2c). More importantly, when the MCs were analyzed by means of fluorescence microscopy below (30 °C) and above (55 °C) DC T_m, two relevant observations were made. First, the MCs preserved their morphology regardless of the state – solid or liquid – of the encapsulated PCM, and no leakage of melted DC outside of the MCs was observed (Figure 2d). Therefore, this demonstrates the impermeability of the highly cross-linked MUF shell. Secondly, the temperature-responsive fluorescence behavior of the bulk DC-dye mixtures was reproduced in the MCs. Thus, a large increase in blue emission was measured for BPEA@DC-MUF upon heating, while a fluorescence color change from red-orange to green was concomitantly registered for PDI@DC-MUF (Figure 2d). These results were corroborated by fluorescence spectrum measurements of the MCs at increasing temperatures from 30 to 55 °C, which also demonstrated that their emission-switching behavior takes place abruptly around DC T_m (Figure 2e). Diffuse reflectance spectra of the MCs obtained at 25 and 55 °C also showed similar absorption changes to the bulk DC-fluorophore mixtures, which are in agreement with the selective aggregation of BPEA and PDI molecules in the solid state of the capsules that account for their thermoreponsive fluorescence behavior (Figure S4, Supporting Information).

To further enhance the dynamic thermoresponsive emission of the 3D codes based on microencapsulated PCM-dye mixtures, we conducted the preparation of BPEA- and PDI-containing MCs presenting emission modulation at different temperatures than DC T_m. For that purpose, paraffins with other melting points were utilized as PCMs. Specifically, octadecane (OD, T_m = 28 °C),[55] tetracosane (TC, T_m = 52 °C)[55] and octacosane (OC, T_m = 60.3 °C)[55] were employed to obtain MCs showing the same fluorescence switching behavior as BPEA@DC-MUF and PDI@DC-MUF but at temperatures around the melting point of the corresponding PCM (**Figure 3**a; Figure S5, Supporting Information). The successful formation of these MCs was verified by SEM imaging (Figure S6, Supporting Information), while DSC analysis demonstrated the encapsulation of the PCMs and the maintenance of their bulk thermal properties (Figure 3b; Figure S7, Supporting Information). Interestingly, when analyzing the thermoinduced fluorescence modulation of all these MCs, we found that it occurs at sufficiently different temperatures for each type of encapsulated PCM to be registered as separable discrete emission variation steps (Figure 3c). This feature is crucial to allow discrimination of MCs loaded with distinct PCMs during the thermal readout of the final 3D codes.

To fabricate each of the thermoresponsive fluorescent pixels that would compose the stimuli-responsive 3D codes, we embedded one type of MC containing each fluorophore within a 2 × 2 × 0.3 mm piece of poly(vinyl alcohol) film (PVA) by drop-casting – for instance, BPEA@DC-MUF and PDI@OC-MUF MCs in the example shown in **Figure** 4a–e. The integration of the capsules within the polymer matrix was confirmed by SEM after analyzing the millimeter-sized pixel's edge, where the presence of several intact capsules was observed (Figure 4b). As a result, the resulting pixel preserved the temperature-dependent emission behavior of its constituting capsules: it showed a fluorescence increment in the blue region at temperatures around DC T_m, and a red-to-green emission switch at temperatures around OC T_m, yielding an overall multistate emitting pixel (Figure 4c). Moreover, the emission changes as well as the PCM thermal transitions responsible for them were found to be completely reversible after several temperature switching cycles (Figure 4d,e; Figures S8–S9, Supporting Information). Therefore, these results clearly demonstrate that the confinement of PCM-fluorophore mixtures in MCs and their posterior dispersion in polymer films is an efficient strategy to directly transfer the thermoresponsive fluorescence behavior of PCM-based systems into robust physical solid supports –, i.e., to preserve the integrity of the information that would be encoded by each PCM-dye mixture loaded within the pixels of our 3D codes. In addition, it is worth noting the low cost, simplicity, and scalability of the materials and technologies used for the fabrication of these pixels, as all their components are readily available (commercial dyes, paraffins, and polymers) and can be assembled through simple and high-throughput techniques (emulsion encapsulation and drop-casting).

Because of the sudden emission modulation exhibited by our dye-paraffin mixtures around their T_m, the thermoreponsive fluorescent pixels can in principle show up to four different emission states only, upon temperature variation –, i.e., four discrete emission colors with distinguishable chromaticity coordinates that arise from the combination of the two possible fluorescence states for each type of capsule in the pixels (Figure S10, Supporting Information). As a result, they are not suitable for encoding analog information,[62] which would require a continuous variation of emission color (or intensity) with temperature, as we have previously described using intrinsic thermosensitive emitters.[58] By contrast, our four-state thermoresponsive fluorescent pixels are specially well-suited for storing digital data. For this application, it would be very convenient that the information encoded within each pixel –, i.e., the state of the loaded capsules – could be unambiguously read by simple digital processing of their fluorescence images. To investigate this behavior, we did not only focus on the pixel containing BPEA@DC-MUF and PDI@OC-MUF MCs, but we also considered another pixel

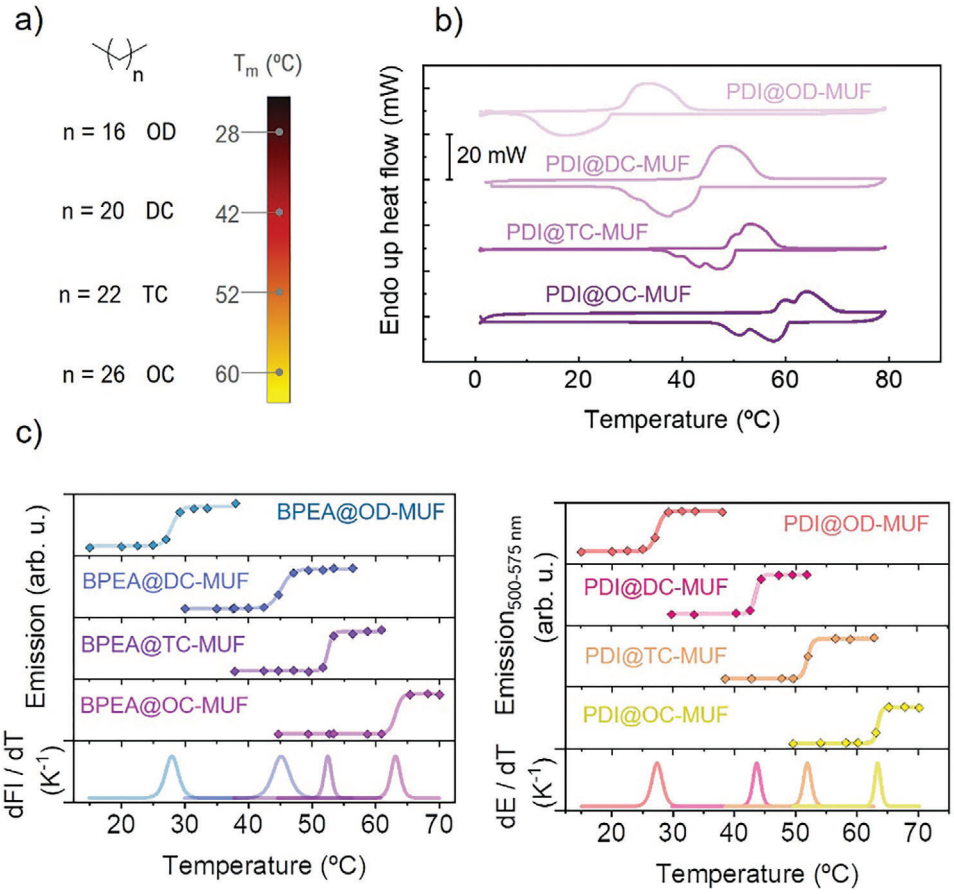

Figure 3. a) Chemical structures and T_m values of the paraffins utilized for the preparation of MCs showing emission switching at different temperatures (OD = octadecane, T_m = 28 °C; DC = docosane, T_m = 42 °C; TC = tetracosane, T_m = 52 °C; OC = octacosane, T_m = 60.3 °C). b) DSC thermograms for the different microencapsulated PDI-paraffins. c) Temperature-induced variation of the emission of thermoresponsive fluorescent MCs containing (left) BPEA and (right) PDI in different PCMs. In the case of off-on switching BPEA-containing MCs, the integral of the emission signal over the whole spectrum is plotted. For PDI-loaded MCs exhibiting on_1-on_2 fluorescence modulation, the signal integrated over the green monomer emission spectrum is selectively plotted (λ_{em} = 500 – 575 nm). The bottom plot of the two graphs shows the derivative of the emission curves (dFl/dT) registered for the thermoresponsive fluorescent MCs, which allows clear identification of the temperatures at which emission changes occur for each paraffin-dye mixture.

loaded with capsules displaying BPEA- and PDI-based emission modulation at the same temperature –, i.e., using the same PCM (BPEA@DC-MUF and PDI@DC-MUF MCs, **Figure 5**). Fluorescence images of these two pixels were acquired with a conventional cell phone camera at increasing temperatures, observing abrupt emission variations when surpassing the melting point of any of the embedded PCMs. Because of the partial overlap between blue BPEA and green PDI monomer emissions, the fluorescence signal was split utilizing optical filters prior to image acquisition ($\lambda_{em} < 532$ nm and $\lambda_{em} > 550$ nm for selective BPEA and PDI emission detection, respectively; Figure S11, Supporting Information). After recording the fluorescence images in these two different spectral ranges, they were separately decomposed into red (R), green (G), and blue (B) channels by digital image processing, with which we aimed to digitally elucidate the state of each fluorophore at the measurement temperature (Figure S12, Supporting Information). In the case of BPEA emission, the intensity of the B and, to a lesser extent, G colors rose after PCM melting due to the increment in dye fluorescence (Figure 5; Figure S13, Supporting Information). For PDI emission, it was the G/R intensity ratio which dramatically varied upon PCM melting, as red excimer-like fluorescence switched into green monomer emission (Figure 5; Figure S13, Supporting Information). Based on these variations in the RGB color space, a simple algorithm was developed to analyze the fluorescence images for each pixel and determine the state of its BPEA- (off or on) and PDI-containing (on_1 or on_2) capsules at each temperature. In this way, fast digital analysis of our 3D codes could be performed to retrieve the data stored.

2.2. 3D Information Encoding with High Encryption Security and 4D Data Storage

After developing the technology for the preparation and the digital readout and processing of thermoresponsive fluorescent pixels, we pursued its application to the realization of advanced data encoding systems. In particular, two different cases were considered: i) 3D information encoding with high encryption security, and ii) 4D information storage.

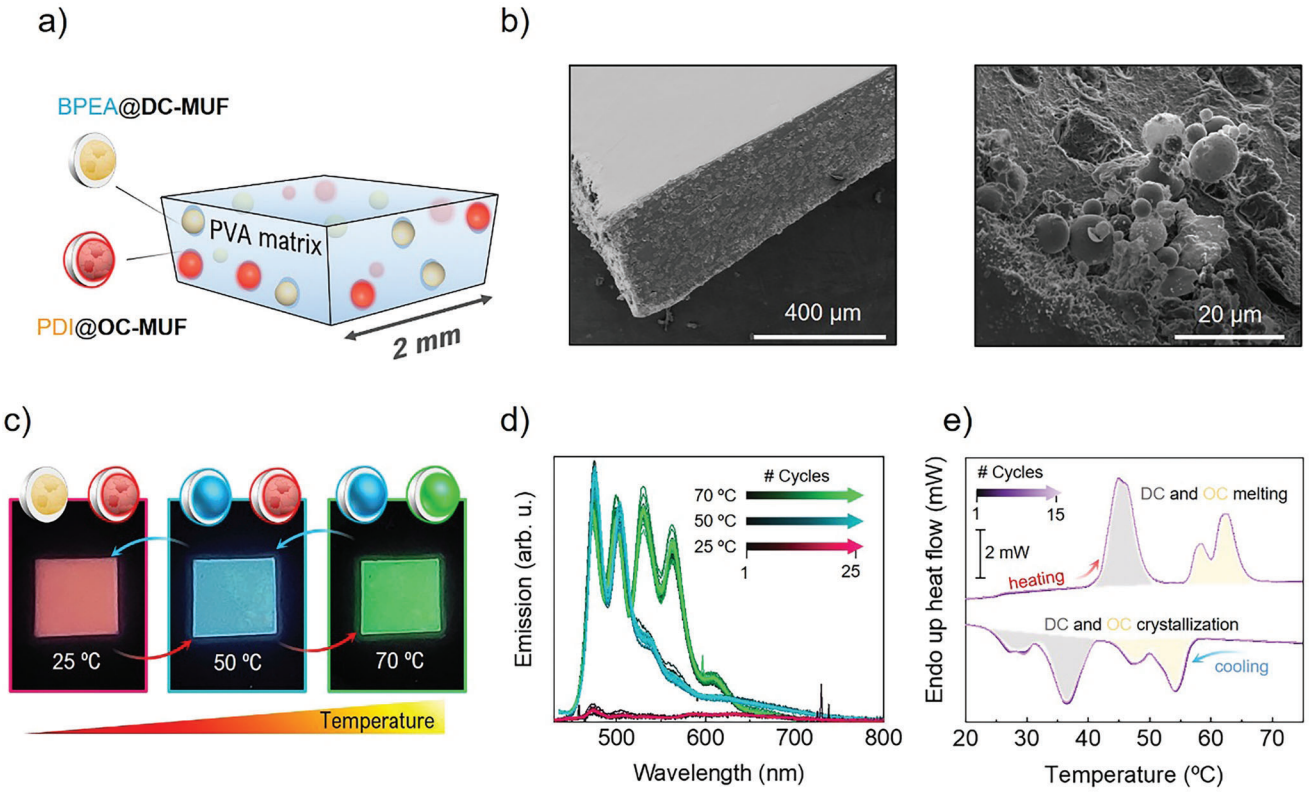

Figure 4. a) Schematic structure of a thermoresponsive pixel, where BPEA@DC-MUF and PDI@OC-MUF MCs are embedded in a PVA matrix. b) SEM images of the thermoresponsive pixel, where many capsules and holes left over by the capsules can be observed on the edges of the PVA film. c) Fluorescence photographs of the thermoresponsive pixel at its three different emission states, where BPEA@DC-MUF and PDI@OC-MUF MCs are both in the solid state (25 °C), ones in the liquid state and the others in the solid state (50 °C), and both in the liquid state (70 °C). The MCs cartoons indicate the fluorescent state of the capsules at each temperature (left: BPEA@DC-MUF; right: PDI@OC-MUF). d) Emission spectra of the thermoresponsive pixel at 25, 50, and 70 °C during 25 consecutive heating-cooling cycles. e) DSC thermograms of the thermoresponsive pixel during 15 consecutive heating-cooling cycles.

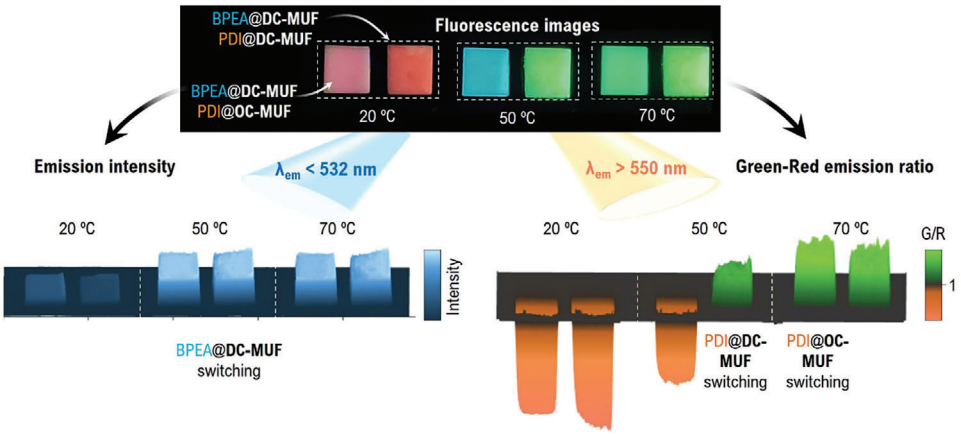

Figure 5. (top) Fluorescence photographs of two thermoresponsive pixels of different compositions at three distinct temperatures: 20 °C (DC and OC solid), 50 °C (DC melted and OC solid), and 70 °C (DC and OC melted). (bottom) Intensity maps of the digital RGB decomposition of these fluorescence images at 20, 50, and 70 °C, which were acquired into two different spectral ranges: λ_{em} < 532 nm (for selective BPEA detection) and λ_{em} > 550 nm (for selective PDI detection). For the images at λ_{em} < 532 nm, the added intensity of their B and G channels is given, which correlates with the off-on emission switch of the BPEA-containing MCs of the pixels. For the images at λ_{em} > 550 nm, the intensity ratio between the G and R channels is instead provided, which evidences the on_1-on_2 emission modulation of PDI-containing MCs.

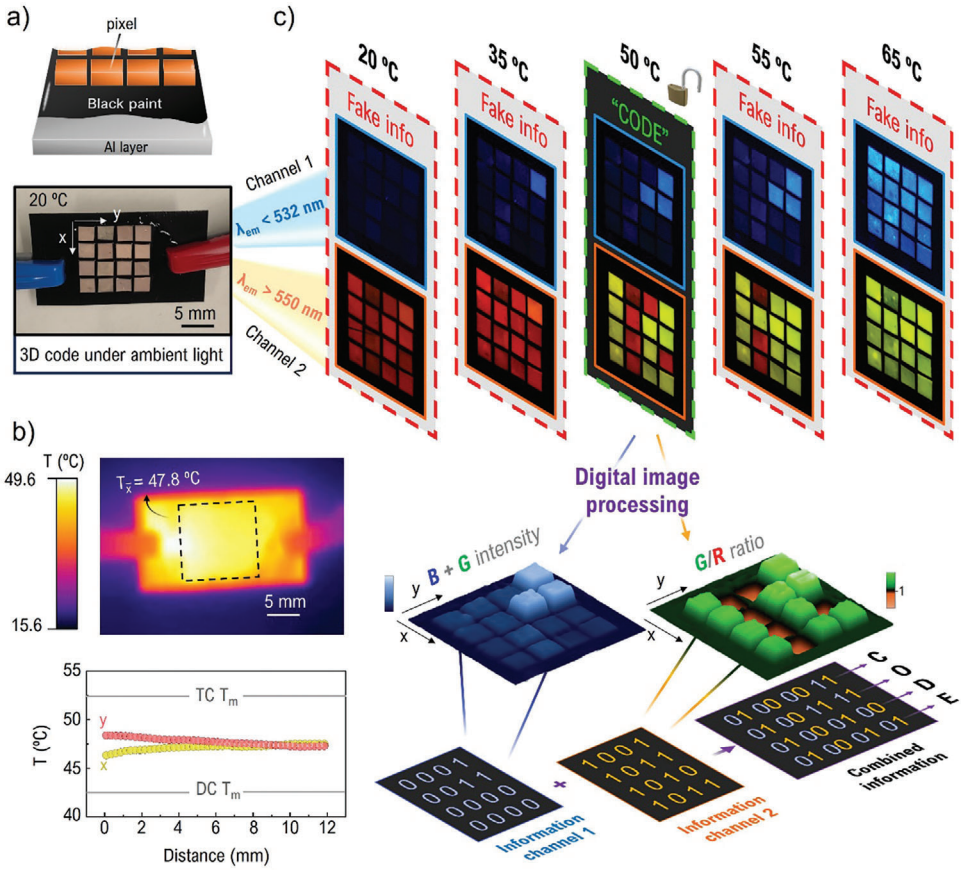

Figure 6. a) Scheme and image under ambient light of the 4 × 4 array of pixels designed to demonstrate 3D information encoding with high-security encryption. b) (top) Thermal image of the device when applying 30 mV to the aluminum support, which resulted in a rather homogeneous temperature ≈ 47.8 °C. The dashed square shows the area of the device where the array of pixels is confined. (bottom) Graph of the temperature distribution along the x- and y-axis of the pixel array for an applied voltage of 30 mV. c) (top) Fluorescence images of the 3D code acquired at different temperatures in two different detection channels (channel 1: λ_{em} < 532 nm; channel 2: λ_{em} > 550 nm). (bottom) Intensity maps of the RGB-decomposed fluorescent images at 50 °C, where the intensity of the B+G channels and the G/R channel ratio were used to recover the bit values associated with the state of the BPEA- and PDI-containing MCs in each pixel, respectively ("0" for low B+G intensity and G/R ratio lower than 1; "1" for high B+G intensity and G/R ratio higher than 1). This digital information combined allowed decrypting the word "CODE".

For the first of these systems, we explored the fabrication of a thermoresponsive 3D code where the true information stored could only be read at a very specific range of temperatures. This should provide high protection to the data encoded, as it could only be accessed if the appropriate readout temperature is known. To this goal, we used a base-2 code system to store binary data in our thermoresponsive fluorescent MCs, where their emission in the solid state encodes the bit "0" while their fluorescence in the liquid state encodes the bit "1". Since our pixels contain two different types of MCs (containing different fluorophores), this implies that each of them encodes a 2-bit value ("00", "01", "10" or "11"). By convention, we assigned the first digit of these values to the information stored in BPEA-containing MCs, while the second was associated with the data encoded in PDI-based MCs.

To demonstrate 3D encoding with high-security encryption, a 4 × 4 thermoresponsive pixel array was fabricated and attached to a thin aluminum layer (≈ 200 µm) previously painted in black (**Figure** 6a). This allowed us to homogeneously vary the temperature of the pixel array in a controlled fashion thanks to the electrothermal heating generated when applying an electrical voltage to the aluminum layer (Figure 6b; Figure S14, Supporting Information). According to the encryption system described above, the composition of the pixel array –, i.e., the nature of the MCs embedded in each pixel – was designed to represent the word "CODE" in binary form only when its fluorescence was measured at temperatures between 45 and 55 °C (C = "01000011", O = "01001111", D = "01000100", E = "01000101"). By contrast, other false information would be retrieved if the emission of the pixel array was registered at temperatures below or above this range. The experimental realization of this concept is shown in Figure 6c while the capsules' pair types employed for each pixel are shown in Figure S15 (Supporting Information). First, the fluorescence images of our 4 × 4-pixel array were measured in two different detection channels (channel 1: λ_{em} < 532 nm; channel 2: λ_{em} >550 nm) and at distinct temperatures accomplished electrothermally (20, 35, 50, 55, and 65 °C). As expected, the BPEA- and PDI-containing MCs of the pixels showed abrupt emission changes when the temperature reached the T_m of the encapsulated PCM, which were fully preserved upon sequential

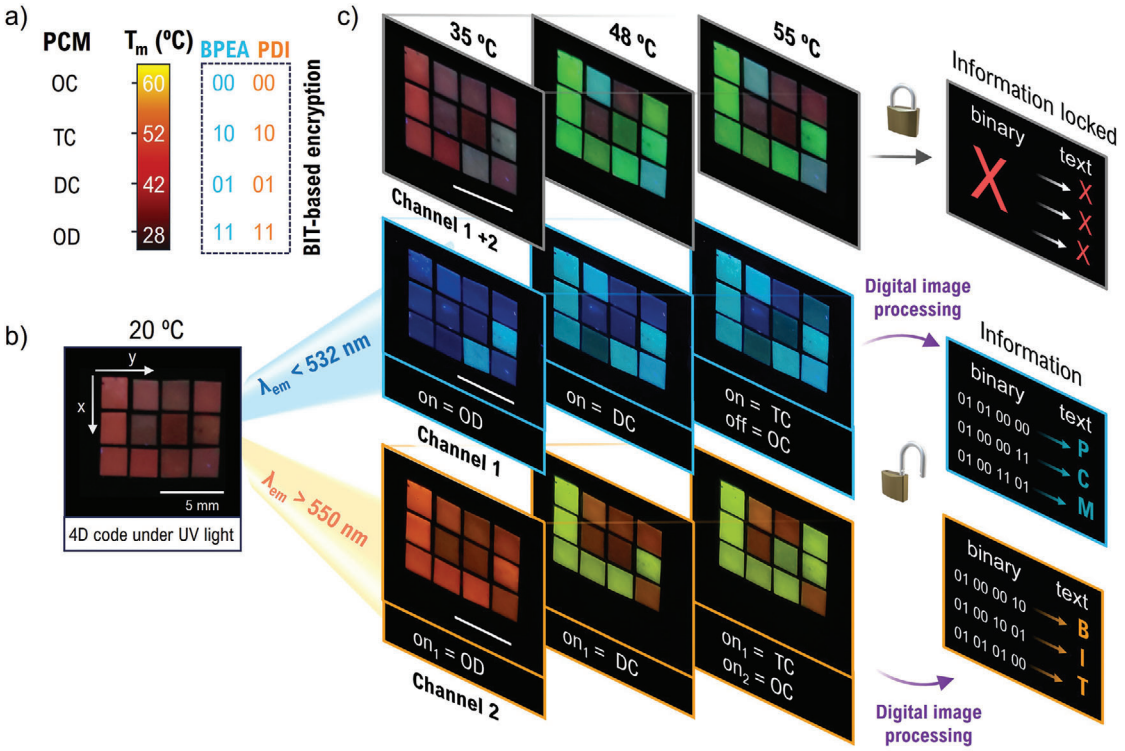

Figure 7. a) Encoding system for 4D data storage where information is additionally encrypted in the thermal dimension according to the T_m of four paraffin PCMs. The 8 types of MCs that can be prepared from these PCMs and the dyes BPEA and PDI are the base for the two independent encryption systems of our design. b) Fluorescence image at 20 °C of the 3 × 4 array of pixels composing the code for 4D information storage. c) Fluorescence images of the pixel array acquired at the three temperatures of interest without spectral filtering (first row), with a 532 SP filter to selectively detect BPEA emission in the λ_{em} < 532 nm channel (second row), and with a 550 LP filter to selectively read PDI emission in the λ_{em} > 550 nm channel (third row). After the digital RGB decomposition of these images and analysis of their B+G and G/R ratio channels, the binary codes for the words "PCM" and "BIT" were recovered.

heating-cooling cycles and storage under ambient conditions for several months (Figure S16a, Supporting Information). As a result, the 3D code displayed five different fluorescent states and, consequently, five different information readouts. Finally, by digitally processing the fluorescence images taken at each temperature using RGB decomposition, two matrices of binary coding were obtained at each temperature (or applied voltage). The combination of the two matrices has been arbitrarily implemented as the sequential reading of one pixel of the channel 1 matrix and one pixel of the channel 2 matrix. In this way the encrypted word "CODE" could only be deciphered when analyzing the emission of the 3D code at 50 °C.

In a second step, we developed a different encoding device to demonstrate the potential of our thermoresponsive fluorescent 3D codes to enable true 4D data storage. For this, we employed a code system where we assigned a pair of bits to each PCM contained in our MCs (OD = "11", DC = "01", TC = "10", and OC = "00") –, i.e., four states were possible for each MC in the pixels (**Figure** 7a). Therefore, in this case, information was not associated with the fluorescent state of the MCs (off-on or on_1-on_2), but with the nature of the encapsulated PCMs in each pixel, which can be determined by measuring their thermoresponsive emission behavior. It must be mentioned that the different melting points of encapsulated inorganic PCMs have been previously exploited to obtain thermal barcoded information, where, however, its reading had to be carried out through DSC measurements.[63,64] Our encapsulated fluorophore-PCM mixtures allow for easy and remote detection of the fluorescent state through optical detection. In addition, it allows data to be stored in the resulting pixel array in 4D: two spatial dimensions (the x and y positions of each pixel in the array); one color dimension (the separate blue and red-green emissions from BPEA- and PDI-based MCs, respectively); and one temperature dimension (the T_m of the encapsulated PCM). Consequently, reading the information encoded in the thermal dimension would require registering the emission of the array of pixels at different temperatures – in particular, at three intermediate temperatures between OD and OC melting points.

To implement this strategy toward 4D data storage, we prepared a 3 × 4-pixel array where two different words were encoded in binary format for each emission channel: "PCM" (P = "01010000", C = "01000011", M = "01001101") for λ_{em} < 532 nm from BPEA-containing MCs, and "BIT" (B = "01000010", I = "01001010", T = "01010100") for λ_{em} > 550 nm from PDI-based MCs (Figure 7b). To read this information, the two-channel fluorescence images of the array were recorded at different temperatures using electrothermal heating and analyzed utilizing the same digital image processing method described above (Figure 7c; Figures S17–S18 and Movie S1, Supporting Information). In this case, however, "11", "01", "10" or "00" values were

assigned to the two emission channels of each pixel depending on the melting temperature of the PCM within the BPEA- and PDI-loaded capsules. The main advantages of this 4D encoding system are multifold. First, the four PCM-based systems used admit storing the double of information bits per pixel relative to a conventional two-emission channel 3D luminescent code. Second, the need to acquire the emission from the pixel array at different defined temperatures for readout makes the encoded data more secure and protected. Third, when compared to previous reports where time-dependent luminescent changes were utilized to accomplish 4D data storage,[35,41–43] the use of temperature as the fourth dimension makes the readout process reproducible regardless of the operation conditions (e.g., temperature scanning direction and rate, external temperature). In addition, the thermoresponsive emission behavior of our pixel array remains invariant upon repetitive temperature scans and storage for prolonged periods under ambient conditions, thus allowing for multiple readout processes in time without damaging the information encoded (Figure S16b, Supporting Information). Finally, as the T_m values of the utilized PCMs are relatively close and fluorescence measurements only need to be taken at three intermediate temperatures to determine the whole composition of the array, the readout process through thermal scanning should not be excessively time-consuming (Movie S1, Supporting Information).

3. Conclusion

In summary, we have demonstrated herein a novel strategy for the preparation of stimuli-responsive 3D codes for information encoding and storage based on microencapsulated thermoresponsive PCM-fluorophore mixtures. By mixing capsules made from different dyes –, i.e., with distinct emission colors – and PCMs –, i.e., suffering abrupt fluorescence variation at different temperatures – within transparent polymer films, 2D-pixel arrays could be prepared that exhibited dynamic multichannel emission behavior upon temperature changes that could be easily processed digitally. As a result, advanced digital encoding operations could be realized that are hard to replicate with other stimuli-responsive luminescent materials. First, thermoresponsive 3D codes were prepared showing a high level of encryption security, as the true encoded information could only be read at a defined range of temperatures. Second, by exploiting the thermal dimension to encrypt information, our thermoresponsive pixel arrays could be endowed with real 4D data storage capabilities. In combination with the low cost, facility, and scalability of the fabrication process of thermoresponsive fluorescent pixels based on encapsulated PCM-dye mixtures, these results validate the potential of our novel technology for fluorescent data encoding and storage. Future research should face the miniaturization of the pixels as well as the use of more emitters with narrower emission bands or more PCMs with different melting points, which would further enhance the data density performance of our stimuli-responsive 3D codes.

Supporting Information

Supporting Information is available from the Wiley Online Library or from the author.

Acknowledgements

This work was supported by grants PID2021-127983OB-C21 and PID2022-141293OB-I00 funded by MICIU/AEI/10.13039/501100011033 and by ERDF – "A way of making Europe". The ICN2 is supported by the Severo Ochoa Centres of Excellence program, Grant CEX2021-001214-S, funded by MICIU/AEI/10.13039.501100011033. UAB thanks the support from Generalitat de Catalunya (2021 SGR 00064 project). J.R.O. thanks the Generalitat de Catalunya (AGAUR) for his predoctoral FI fellowship.

Conflict of interest

The authors declare no conflict of interest.

Data Availability Statement

The data that support the findings of this study are openly available in CORA.RDR at https://dataverse.csuc.cat.

Keywords

anticounterfeiting, emission modulation, encoding, optical data storage, phase change materials

Received: February 8, 2024
Revised: March 19, 2024
Published online:

[1] A. Abdollahi, H. Roghani-Mamaqani, B. Razavi, M. Salami-Kalajahi, *ACS Nano* **2020**, *14*, 14417.
[2] P. Kumar, S. Singh, B. K. Gupta, *Nanoscale* **2016**, *8*, 14297.
[3] Y. Shen, X. Le, Y. Wu, T. Chen, *Chem. Soc. Rev.* **2024**, *53*, 606.
[4] H. Suo, Q. Zhu, X. Zhang, B. Chen, J. Chen, F. Wang, *Mater. Today Phys.* **2021**, *21*, 100520.
[5] K. Muthamma, D. Sunil, P. Shetty, *Mater. Today Chem.* **2020**, *18*, 100361.
[6] W. Ren, G. Lin, C. Clarke, J. Zhou, D. Jin, *Adv. Mater.* **2020**, *32*, 1901430.
[7] H. Zhou, J. Han, J. Cuan, Y. Zhou, *Chem. Eng. J.* **2022**, *431*, 134170.
[8] X. Yu, H. Zhang, J. Yu, *Aggregate* **2021**, *2*, 20.
[9] H. Wang, X. Ji, Z. A. Page, J. L. Sessler, *Mater. Chem. Front.* **2020**, *4*, 1024.
[10] D.-H. Park, C. J. Han, Y.-G. Shul, J.-H. Choy, *Sci. Rep.* **2014**, *4*, 4879.
[11] X. Ji, R.-T. Wu, L. Long, X.-S. Ke, C. Guo, Y.-J. Ghang, V. M. Lynch, F. Huang, J. L. Sessler, *Adv. Mater.* **2018**, *30*, 1705480.
[12] J. Sun, J. Wang, M. Chen, X. Pu, G. Wang, L. Li, G. Chen, Y. Cai, X. Gu, B. Z. Tang, *Chem. Mater.* **2019**, *31*, 5683.
[13] J. W. Oh, S. Lee, H. Han, O. Allam, J. I. Choi, H. Lee, W. Jiang, J. Jang, G. Kim, S. Mun, K. Lee, Y. Kim, J. W. Park, S. Lee, S. S. Jang, C. Park, *Light Sci. Appl.* **2023**, *12*, 226.
[14] Y.-M. Wang, X.-T. Tian, H. Zhang, Z.-R. Yang, X.-B. Yin, *ACS Appl. Mater. Interfaces* **2018**, *10*, 22445.
[15] S. Wei, Z. Li, W. Lu, H. Liu, J. Zhang, T. Chen, B. Z. Tang, *Angew. Chem., Int. Ed.* **2021**, *60*, 8608.
[16] A. A. Nagarkar, S. E. Root, M. J. Fink, A. S. Ten, B. J. Cafferty, D. S. Richardson, M. Mrksich, G. M. Whitesides, *ACS Cent. Sci.* **2021**, *7*, 1728.
[17] Z. Quan, Q. Zhang, H. Li, S. Sun, Y. Xu, *Coord. Chem. Rev.* **2023**, *493*, 215287.
[18] H. Zhang, X. Guo, K. Jian, L. Fu, X. Zhao, *Inorg. Chem.* **2023**, *62*, 13847.

[19] Z. Li, R. Núñez, M. E. Light, E. Ruiz, F. Teixidor, C. Viñas, D. Ruiz-Molina, C. Roscini, J. G. Planas, *Chem. Mater.* **2022**, *34*, 4795.
[20] K. Lou, Z. Hu, H. Zhang, Q. Li, X. Ji, *Adv. Funct. Mater.* **2022**, *32*, 2113274.
[21] X. Ji, Z. Li, X. Liu, H.-Q. Peng, F. Song, J. Qi, J. W. Y. Lam, L. Long, J. L. Sessler, B. Z. Tang, *Adv. Mater.* **2019**, *31*, 1902365.
[22] X. Ji, W. Chen, L. Long, F. Huang, J. L. Sessler, *Chem. Sci.* **2018**, *9*, 7746.
[23] Z. Li, H. Chen, B. Li, Y. Xie, X. Gong, X. Liu, H. Li, Y. Zhao, *Adv. Sci.* **2019**, *6*, 1901529.
[24] H. Shi, S. Wu, M. Si, S. Wei, G. Lin, H. Liu, W. Xie, W. Lu, T. Chen, *Adv. Mater.* **2022**, *34*, 2107452.
[25] Y. Liu, M. Li, H. Ju, Z. Wang, Y. Wu, Z. L. Wu, H. Zhu, F. Huang, *Polym. Chem.* **2022**, *13*, 6255.
[26] Y. Wu, X. Chen, W. Wu, *Small* **2023**, *19*, 2206709.
[27] W. Lu, M. Si, H. Liu, H. Qiu, S. Wei, B. Wu, R. Wang, G. Yin, J. Zhang, P. Theato, Y. Wei, T. Chen, *Cell Rep. Phys. Sci.* **2021**, *2*, 100417.
[28] J. Deng, H. Wu, W. Xie, H. Jia, Z. Xia, H. Wang, *ACS Appl. Mater. Interfaces* **2021**, *13*, 39967.
[29] X. Zhang, Y. Cheng, J. You, J. Zhang, Y. Wang, J. Zhang, *ACS Appl. Mater. Interfaces* **2022**, *14*, 16582.
[30] F. Miller, S. Wintzheimer, J. Prieschl, V. Strauss, K. Mandel, *Adv. Opt. Mater.* **2021**, *9*, 2001972.
[31] L. Lu, K. Wang, H. Wu, A. Qin, B. Z. Tang, *Chem. Sci.* **2021**, *12*, 7058.
[32] Z. Gao, Z. Chen, Y. Han, F. Wang, *Nanoscale Horiz.* **2020**, *5*, 1081.
[33] Y. Zhang, X. Le, Y. Jian, W. Lu, J. Zhang, T. Chen, *Adv. Funct. Mater.* **2019**, *29*, 1905514.
[34] H. Zhang, Q. Li, Y. Yang, X. Ji, J. L. Sessler, *J. Am. Chem. Soc.* **2021**, *143*, 18635.
[35] Y.-D. Yang, X. Ji, Z.-H. Lu, J. Yang, C. Gao, H. Zhang, B. Z. Tang, J. L. Sessler, H.-Y. Gong, *Nat. Commun.* **2020**, *11*, 77.
[36] M. Tu, H. Reinsch, S. Rodríguez-Hermida, R. Verbeke, T. Stassin, W. Egger, M. Dickmann, B. Dieu, J. Hofkens, I. F. J. Vankelecom, N. Stock, R. Ameloot, *Angew. Chem., Int. Ed.* **2019**, *131*, 2445.
[37] Y. Li, D. J Young, X. Jun Loh, *Mater. Chem. Front.* **2019**, *3*, 1489.
[38] D. Lu, M. Zhu, S. Wu, Q. Lian, W. Wang, D. Adlam, J. A. Hoyland, B. R. Saunders, *Adv. Funct. Mater.* **2020**, *30*, 1909359.
[39] L. Popa, M. V. Ghica, C. Dinu-Pirvu, *Hydrogels: Smart Materials for Biomedical Applications*, IntechOpen, London, England **2019.**
[40] H. Liu, S. Wei, H. Qiu, M. Si, G. Lin, Z. Lei, W. Lu, L. Zhou, T. Chen, *Adv. Funct. Mater.* **2022**, *32*, 2108830.
[41] H. Xie, Z. Li, J. Gong, L. Hu, P. Alam, X. Ji, Y. Hu, J. H. C. Chau, J. W. Y. Lam, R. T. K. Kwok, B. Z. Tang, *Adv. Mater.* **2021**, *33*, 2105113.
[42] X. Wang, H. Ma, M. Gu, C. Lin, N. Gan, Z. Xie, H. Wang, L. Bian, L. Fu, S. Cai, Z. Chi, W. Yao, Z. An, H. Shi, W. Huang, *Chem. Mater.* **2019**, *31*, 5584.
[43] J. Tan, Q. Li, S. Meng, Y. Li, J. Yang, Y. Ye, Z. Tang, S. Qu, X. Ren, *Adv. Mater.* **2021**, *33*, 2006781.
[44] J. Du, L. Sheng, Y. Xu, Q. Chen, C. Gu, M. Li, S. X.-A. Zhang, *Adv. Mater.* **2021**, *33*, 2008055.
[45] W. Zhang, X. Ji, B.-J. Peng, S. Che, F. Ge, W. Liu, M. Al-Hashimi, C. Wang, L. Fang, *Adv. Funct. Mater.* **2020**, *30*, 1906463.
[46] J. Du, L. Sheng, Q. Chen, Y. Xu, W. Li, X. Wang, M. Li, S. X.-A. Zhang, *Mater. Horiz.* **2019**, *6*, 1654.
[47] C. Bellacanzone, J. R. Otaegui, J. Hernando, D. Ruiz-Molina, C. Roscini, *Adv. Opt. Mater.* **2022**, *10*, 2102423.
[48] J. R. Otaegui, P. Rubirola, D. Ruiz-Molina, J. Hernando, C. Roscini, *Adv. Opt. Mater.* **2020**, *8*, 2001063.
[49] K. Xue, C. Wang, J. Wang, S. Lv, B. Hao, C. Zhu, B. Z. Tang, *J. Am. Chem. Soc.* **2021**, *143*, 14147.
[50] J. R. Otaegui, D. Ruiz-Molina, L. Latterini, J. Hernando, C. Roscini, *Mater. Horiz.* **2021**, *8*, 3043.
[51] K. Zhang, X. Zhou, S. Li, L. Zhao, W. Hu, A. Cai, Y. Zeng, Q. Wang, M. Wu, G. Li, J. Liu, H. Ji, Y. Qin, L. Wu, *Adv. Mater.* **2023**, *35*, 2305472.
[52] J. R. Otaegui, A. Carrascull-Marín, D. Ruiz-Molina, J. Hernando, C. Roscini, *Adv. Opt. Mater.* **2022**, *10*, 2200083.
[53] W. Feng, Y. Wu, D. Chen, S. Lu, Y. Zhao, H. Yan, *Chem. Commun.* **2023**, *59*, 14823.
[54] Y.-J. Jin, R. Dogra, I. W. Cheong, G. Kwak, *ACS Appl. Mater. Interfaces* **2015**, *7*, 14485.
[55] A. H. Johnstone, *CRC Handbook of Chemistry and Physics—69th Edition Editor in Chief R. C. Weast*, CRC Press Inc., Boca Raton, Florida **1988**.
[56] C. Shang, G. Wang, Y.-C. Wei, Q. Jiang, K. Liu, M. Zhang, Y.-Y. Chen, X. Chang, F. Liu, S. Yin, P.-T. Chou, Y. Fang, *CCS Chem.* **2021**, *4*, 1949.
[57] Y. J. Bae, G. Kang, C. D. Malliakas, J. N. Nelson, J. Zhou, R. M. Young, Y.-L. Wu, R. P. Van Duyne, G. C. Schatz, M. R. Wasielewski, *J. Am. Chem. Soc.* **2018**, *140*, 15140.
[58] N. A. Vázquez-Mera, J. R. Otaegui, R. S. Sánchez, G. Prats, G. Guirado, D. Ruiz-Molina, C. Roscini, J. Hernando, *ACS Appl. Mater. Interfaces* **2019**, *11*, 17751.
[59] M. A. White, M. LeBlanc, *J. Chem. Educ.* **1999**, *76*, 1201.
[60] A. Hakami, S. S. Srinivasan, P. K. Biswas, A. Krishnegowda, S. L. Wallen, E. K. Stefanakos, *J. Coat. Technol. Res.* **2022**, *19*, 377.
[61] S. Han, Y. Chen, S. Lyu, Z. Chen, S. Wang, F. Fu, *Colloids Surf A Physicochem Eng Asp* **2020**, *585*, 124046.
[62] G. Copley, T. A. Moore, A. L. Moore, D. Gust, *Adv. Mater.* **2013**, *25*, 456.
[63] M. Zare, K. S. Mikkonen, *Adv. Funct. Mater.* **2023**, *33*, 2213455.
[64] Z. Ma, Y. Hong, M. Zhang, M. Su, *Appl. Phys. Lett.* **2009**, *95*, 233101.